# Endothelial Nitric Oxide Synthase: Modulations of the Distal Heme Site Produced by Progressive N-Terminal Deletions†

Ignacio Rodríguez-Crespo,‡ Pierre Moënne-Loccoz,§ Thomas M. Loehr,§ and Paul R. Ortiz de Montellano*,‡

*Department of Pharmaceutical Chemistry, School of Pharmacy, University of California, San Francisco, California 94143-0446, and Department of Chemistry, Biochemistry, and Molecular Biology, Oregon Graduate Institute of Science and Technology, PO Box 91000, Portland, Oregon 97291-1000*

*Received January 27, 1997; Revised Manuscript Received May 13, 1997*⊗

ABSTRACT: cDNAs coding for bovine endothelial nitric oxide synthase (eNOS) with N-terminal deletions of 52, 91, and 105 amino acids were constructed, and the proteins were expressed in *Escherichia coli* and purified by affinity chromatography. All three truncated proteins bind heme and exhibit the ferrous-CO absorption maximum at 444 nm characteristic of thiolate heme ligation. Deletion of the first 52 amino acids yields a fully active dimeric protein with the same spectroscopic properties as the wild-type. The myristoylation, palmitoylation, and polyproline domains of the enzyme located in the deleted region are therefore not required for full catalytic activity. The $\Delta^{91}$ and $\Delta^{105}$ proteins, which exhibit altered dimerization equilibria, retain 20 and 12%, respectively, of the maximal activity. Resonance Raman and UV−vis spectroscopy indicate that, in the absence of tetrahydrobiopterin ($H_4B$) and L-Arg, the wild-type and $\Delta^{52}$ proteins are predominantly five coordinate high spin, whereas the $\Delta^{91}$ and $\Delta^{105}$ proteins are six coordinate low spin. The $\Delta^{91}$ and $\Delta^{105}$ mutants bind $H_4B$, as indicated by a concomitant decrease in the low-spin component of the UV−vis spectrum, but the binding of L-Arg is extremely slow (∼15 min). Dithiothreitol readily coordinates as the sixth iron ligand in the $\Delta^{91}$ and $\Delta^{105}$ mutants but not in the $\Delta^{52}$ or wild-type proteins. The dithiothreitol can be completely displaced by L-Arg but not by $H_4B$. Resonance Raman comparison of wild-type eNOS and nNOS confirms that, in the absence of $H_4B$ and L-Arg, eNOS is primarily high spin whereas nNOS is predominantly six coordinate, low spin. The results indicate that Cys-101 is not critical for the binding of $H_4B$ and imply that some of the protein residues involved in dimer formation and in preservation of active site integrity are located, probably at the monomer−monomer interface, in the N-terminal end of the protein.

Nitric oxide synthases (NOS)[1] are self-sufficient monooxygenases that synthesize nitric oxide (NO) by converting L-Arg to citrulline using NADPH as the source of electrons (Griffith & Stuehr, 1995; Marletta, 1994; Knowles & Moncada, 1994; Masters, 1994; Bredt & Snyder, 1994). The synthesis of nitric oxide requires dimerization of two NOS polypeptide chains, as only the homodimer is active. Additionally, the protein architecture of the known mammalian NOS enzymes consists of two domains. The oxygenase domain contains a thiolate-ligated heme group and binds both L-Arg and $H_4B$. The reductase domain, which provides electrons to the heme group during catalytic turnover, contains two flavin moieties and a binding site for NADPH. The two domains are separated by a linker peptide with a consensus CaM-binding sequence.

The concentration and site of production of nitric oxide are tightly controlled, owing to the reactivity of this radical. In the constitutive isoforms, binding of CaM in the presence of $Ca^{2+}$ activates electron transfer from the reductase domain to the heme, initiating the production of NO. In the inducible isoform, CaM is always bound to the interdomain hinge and the enzyme activity is regulated at the transcriptional level (Griffith & Stuehr, 1995; Marletta, 1994; Knowles & Moncada, 1994; Masters, 1994; Bredt & Snyder, 1994). Regulation of NO synthesis by mammalian cells also relies on an efficient subcellular localization of the different NOS isoforms in response to various stimuli. The N-terminal regions of all three mammalian nitric oxide synthase isoforms (endothelial, inducible, and neuronal) are implicated in this subcellular targeting. Neuronal NOS is unique in that it contains an extended N-terminal GLGF domain that interacts directly with skeletal muscle dystrophin. This association is responsible for localization of the enzyme in the myocyte sarcolemma of fast-twitch fibers (Brenman et al., 1995). Cell transfection with a mutant nNOS in which the first 226 amino acids have been deleted renders full wild-type nNOS activity with similar $K_m$ and $V_{max}$ values. Clearly, this protein segment is not involved in the catalytic function of the enzyme. Interestingly, this truncated nNOS is almost identical in size to eNOS (Brenman et al., 1995). In contrast, a particulate and a soluble iNOS with differences in their

† This work was supported by National Institutes of Health Grants GM 25515 (P.R.O.M.) and GM 34468 (T.M.L.). Support for the Liver Center core facilities used in the study was provided by Grant 5 P30 DK 26743. I.R-C. is a recipient of a postdoctoral fellowship from the Spanish "Ministerio de Investigacion y Ciencia".

* Author to whom correspondence should be addressed. Fax: (415) 502-4728. Email: ortiz@cgl.ucsf.edu.

‡ University of California.

§ Oregon Graduate Institute of Science and Technology.

⊗ Abstract published in *Advance ACS Abstracts,* July 1, 1997.

[1] Abbreviations: NOS, nitric oxide synthase; eNOS, endothelial NOS; nNOS, neuronal NOS; iNOS, inducible NOS; heme, iron protoporphyrin IX regardless of the iron oxidation or ligation state; L-Arg, L-arginine; $H_4B$; (6*R*)-5,6,7,8-tetrahydrobiopterin; CaM, $Ca^{2+}$-dependent calmodulin; FPLC, fast protein liquid chromatography; HS, high spin; LS, low spin; DTT, dithiothreitol; NTA, nitrilotriacetic acid; RR, resonance Raman; SDS−PAGE, sodium dodecyl sulfate−polyacrylamide gel electrophoresis; UV−vis, ultraviolet−visible.

S0006-2960(97)00192-X CCC: $14.00 

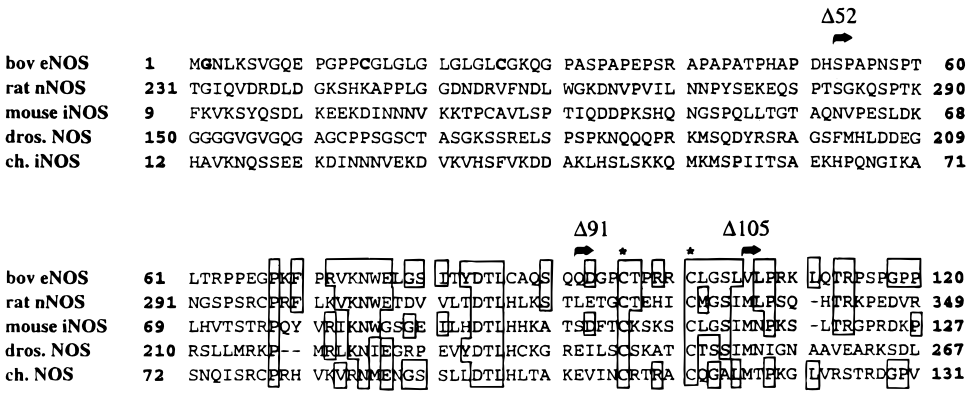


FIGURE 1: Sequence alignment of the deduced amino acid sequences of the N-terminal regions of several NOS isoforms: bovine endothelial NOS (Sessa et al., 1992), rat neuronal NOS (Bredt et al., 1991) and mouse inducible NOS (Xie et al., 1992), drosophila NOS (Regulski & Tully, 1995) and chicken inducible NOS (Lin et al., 1996). The sites of myristoylation (Gly-2) and palmitoylation (Cys-15 and Cys-26) are in bold. The sites of initiation of translation for deletion mutants $\Delta^{52}$, $\Delta^{91}$, and $\Delta^{105}$ are marked with arrows. Identical residues are cased. The stars are positioned on top of the two conserved Cys residues (Cys-96 and Cys-101).

N-termini have been identified in macrophage cells (Ringheim & Pan, 1995). Antibodies elicited against a 17 amino acid polypeptide of the N-terminus of the soluble form did not cross-react with the particulate enzyme (Ringheim & Pan, 1995). However, both forms share immunoreactivity against their C-terminal region. To our knowledge, the exact nature of the N-terminal modification responsible for targeting the iNOS to the particulate fraction has not been identified.

Michel and Sessa have unequivocally established that eNOS is acylated by both N-terminal myristoylation and cysteine palmitoylation. Irreversible myristoylation probably occurs cotranslationally at the N-terminal glycine residue and is required for membrane association (Busconi & Michel, 1993; Sessa et al., 1993). Palmitoylation at cysteine residues 15 and/or 26 targets the enzyme to the plasmalemmal caveolae (Shaul et al., 1996; Liu et al., 1996). Interestingly, palmitoylation-deficient mutants display diminished NO production when compared to wild-type transfected HEK 293 cells, indicating that correct subcellular localization is necessary for efficient cellular NO synthesis (Liu et al., 1996).

In this work, we have performed three progressive N-terminal deletions in eNOS to determine the minimal protein length required for full catalytic activity and efficient NO production. The proteins were expressed in *Escherichia coli* and purified by affinity chromatography, first by binding to a $Ni^{2+}$-NTA resin through a $(His)_6$-tag at the N-terminus followed by binding to ADP-Sepharose. Deletion of 52 amino acids ($\Delta^{52}$) results in a mutant protein with properties very similar to those of wild-type bovine eNOS. Deletions of either 91 or 105 residues ($\Delta^{91}$ or $\Delta^{105}$) produced mutants with severely altered properties. The low activity of the $\Delta^{91}$ and $\Delta^{105}$ mutants results from alterations on the distal side of the heme and impaired dimer formation.

## EXPERIMENTAL PROCEDURES

*Materials.* L-Arg was obtained from Aldrich (Milwaukee, WI), 2′,5′-ADP Sepharose and calmodulin-Sepharose from Sigma (St. Louis, MO), and (6*R*)-5,6,7,8-tetrahydrobiopterin ($H_4B$) from Alexis Biochemicals (San Diego, CA). Vent polymerase and restriction enzymes were from New England Biolabs (Beverly, MA). DNA purification kits and $Ni^{2+}$-NTA Agarose were purchased from QIAGEN (Chatsworth, CA). Bacto yeast extract, bactotryptone, isopropyl $\beta$-D-thiogalactopyranoside, and DH5$\alpha$ *E. coli* cells were from Gibco BRL (Gaithersburg, MD). BL21 competent cells were from Novagen (Madison, WI). All other reagents and materials were from Sigma.

*Cloning*. The polymerase chain reaction was performed with a proof-reading enzyme (Vent DNA Polymerase) in order to amplify the bovine eNOS gene from the desired new initiation codon up to the unique *Kpn*I site of the gene. The oligos used were 5′-GCGCCAGACCATATGGCA-GCTCCCAAC-3′ for the 5′ end of $\Delta^{52}$, 5′-GCGCAGTC-CCATATGGACGGGCCC-3′ for the 5′ end of $\Delta^{91}$, 5′-CTGGGCTCCCATATGTTGCCCCGG-3′ for the 5′ end of $\Delta^{105}$, and 5′-CAGCCGGTACCTCTGG-3′ covering the *Kpn* I site.

For $\Delta^{52}$, a new *Nde*I site at the initiator Met residue followed by an Ala (GCA codon) residue (second amino acid) was positioned at the 5′ end of the gene; in the other two mutants, only a new *Nde*I site was introduced, and Asp (in $\Delta^{91}$) and Leu (in $\Delta^{105}$) were left as the second amino acids (Figure 1). The PCR products were subsequently double digested with *Nde*I plus *Kpn*I and the gene fragments were ligated into polyHis-pCWeNOS (Rodríguez-Crespo et al., 1996) using the *Nde*I and *Kpn*I sites after excision of the corresponding *Nde*I-*Kpn*I fragment from the wild-type. The resulting $\Delta^{52}$-poly-His pCWeNOS, $\Delta^{91}$-poly-His pC-WeNOS, and $\Delta^{105}$-poly-His pCWeNOS were used to transform BL21(DE3) pLysS competent cells.

*Expression.* Expression was performed in the protease-deficient BL21 strain to minimize protein cleavage, essentially as previously described for the wild-type protein (Rodríguez-Crespo et al., 1996). A set of $4 \times 10$ mL cultures of various polyHis pCWeNOS in Luria broth with 200 $\mu$g/mL of ampicillin were grown overnight and used to inoculate 6 L of 2× YT media (four 2.8 L Fernbach flasks with 1.5 L in each) also containing 200 $\mu$g/mL of ampicillin. The cultures were grown to an $OD_{600}$ of 0.8 and induced with 2 mM isopropyl $\beta$-D-thiogalactopyranoside. The cultures were then grown at 22 °C with aeration at a rotation rate of 210 rpm for 20 h before they were harvested by centrifugation. The $\Delta^{52}$ mutant was grown at 190 rpm and lower aeration to minimize protein cleavage. The cells were frozen as a thin film in plastic bags at −70 °C and stored until the protein was purified.

*Purification*. The purification sequence was typically carried out with the protein from 6 L of culture. Due to the instability of all NOS isoforms, the purification was carried out at 4 °C within a period of 1 day in the presence of 10% glycerol, and the resultant protein was quickly frozen in liquid nitrogen in small aliquots and stored at −70 °C.

The cell pellet was lysed in the presence of protease inhibitors and lysozyme by pulse sonication as previously reported (Rodríguez-Crespo et al., 1996; Gerber & Ortiz de Montellano, 1995). When the protein purification was performed in the presence of $H_4B$, the $H_4B$ concentration was kept at 1 $\mu$M and the DTT concentration at 10 $\mu$M to avoid $Ni^{2+}$ precipitation in the presence of reducing agents. After clearance of the cell debris by ultracentrifugation, the cell lysate was loaded onto a $Ni^{2+}$-NTA column (Rodríguez-Crespo et al., 1996). The recombinant protein, with a $(His)_6$-tag at its amino terminus, was bound by the resin. After loading the lysate, the column was washed with five column volumes of buffer A (50 mM Hepes, pH 7.5, 600 mM NaCl, 0.1 mM phenylmethylsulfonyl fluoride, 1 $\mu$M leupeptin, 1 $\mu$M pepstatin, 1 $\mu$M antipain, 1 $\mu$M $H_4B$, and 10% glycerol) and then with 10 column volumes of buffer A plus 7.5 mM imidazole to remove nonspecifically bound proteins. The desired protein was then eluted with buffer A plus 200 mM imidazole, the colored fractions were pooled, and final concentrations of 20 mM L-Arg, 20 $\mu$M $H_4B$, and 10 mM $\beta$-mercaptoethanol were added. The protein was subsequently loaded onto a 2′,5′-ADP-Sepharose column, and the column was washed with 5 column volumes of buffer A plus 20 mM L-Arg and 10 $\mu$M $H_4B$, followed by 5 column volumes of buffer A plus 10 $\mu$M $H_4B$. The purified protein was finally eluted with 20 mM 2′-AMP in buffer A.

*Gel Filtration Chromatography*. Aliquots of 200 $\mu$L of approximately 1.5 mg/mL eNOS were injected into an LCC 500-plus FPLC System (Pharmacia) equipped with two P-500 pumps and a Superdex HR200 column (Pharmacia). Separation was performed at 25 °C and protein detection was performed at 280 nm. The flow rate was kept at 0.5 mL/min and the buffer consisted of 50 mM Hepes, pH 7.5, 10% glycerol, and 100 mM NaCl. The column void volume was determined with dextran blue and the total volume with potassium ferricyanide. The column was calibrated with proteins from a gel filtration calibration kit (Sigma), including thyroglobulin (669 kDa), apoferritin (443 kDa), $\beta$-amylase (200 kDa), alcohol dehydrogenase (150 kDa), bovine serum albumin (66 kDa), and carbonic anhydrase (29 kDa). Horse myoglobin (17 kDa) was used as a protein standard. The calibration curve was obtained by plotting the $(\upsilon_e - \upsilon_0)/(\upsilon_t - \upsilon_0)$ ratio against the log of the molecular weight, where $\upsilon_e$ is the elution volume of the protein, $\upsilon_0$ is the void volume of the column, and $\upsilon_t$ is the total bed volume of the column.

*SDS−PAGE*. Electrophoresis was carried out at ∼4 °C using a Bio-Rad Mini Protean II system as previously described (Rodríguez-Crespo et al., 1996; Klatt et al., 1995).

*UV−Vis Spectroscopic Analysis.* All the spectra were recorded immediately after protein purification in 1 cm masked cuvettes at 15 °C in a dual-beam Cary 1E spectrophotometer connected to a Lauda circulating water bath.

*Resonance Raman Spectroscopy*. For the RR experiments, samples were diluted in 50 mM Hepes, pH 7.4, 5 mM $\beta$-mercaptoethanol, and 500 mM NaCl, to decrease the glycerol concentration, and reconcentrated to approximately 20 $\mu$M with a Microcon 30 (Amicon) ultrafiltration device. Addition of $H_4B$ (10 $\mu$M) and/or L-Arg (10 mM) was performed on the dilution buffer when desired.

Resonance Raman spectra were obtained on a custom McPherson 2061/207 spectrograph (0.67 m focal length, 2400 groove grating, 6 $cm^{-1}$ spectral resolution) using Kaiser Optical holographic super-notch filters and a Princeton instrument (LN-1100PB) liquid $N_2$-cooled CCD detector. The excitation source was provided by an Innova 302Kr (413 nm) laser, setting the power in order to minimize sample heating and photoreduction (∼1 mW). Spectra were collected using a 90-degree scattering geometry and a 5−10 min accumulation time on samples in glass capillaries at room temperature (Loehr & Sanders-Loehr, 1993). Peak frequencies were calibrated relative to an indene standard and are accurate to ±1 $cm^{-1}$. Optical absorption spectra of the RR samples were obtained on a Perkin-Elmer $\lambda$ 9 spectrophotometer (Loehr & Sanders-Loehr, 1993) to follow the completion of substrate and $H_4B$ binding, and integrity was monitored before and after laser exposure on each sample in its capillary tube.

*Protein Determination.* Protein concentrations were determined by the Bradford protein microassay (Bio-Rad) using bovine serum albumin as a standard. Concentrations of heme-containing NOS were determined from the absorption spectrum of the protein using the extinction coefficient $\epsilon_{400} = 100$ $mM^{-1}$ $cm^{-1}$ for the ferric enzyme.

*Enzyme Assays.* The activities of the protein preparations were determined at 37 °C by measuring the production of NO as determined by the conversion of ferrous hemoglobin to ferric methemoglobin plus nitrate, as previously described (Rodríguez-Crespo et al., 1996). The initial rates of NO production were determined from $\Delta A_{401-411}$ ($\Delta\epsilon_{401-411} = 60$ $mM^{-1}$ $cm^{-1}$).

When the NO production rates of mutants $\Delta^{91}$ and $\Delta^{105}$ were calculated, both 20 mM L-Arg and 10 $\mu$M $H_4B$ were added to the freshly purified protein solutions and the absorbance spectra were checked for a low- to high-spin complete transition. Since the 10 mM $H_4B$ stock solution is prepared in 100 mM DTT, the samples were allowed to incubate in the presence of L-Arg until the peaks corresponding to DTT coordination disappeared. When a complete shift to 395 nm was attained, the protein concentration was calculated according to the $\epsilon_{400} = 100$ $mM^{-1}$ $cm^{-1}$ extinction coefficient, and this same protein solution was tested for activity.

## RESULTS

*Expression of the N-Terminal eNOS Deletion Mutants in E. coli*. The recombinant proteins were purified by sequential affinity chromatography, first by binding to $Ni^{2+}$-NTA through the N-terminal poly-His tag and subsequently by binding to 2′,5′-ADP Sepharose through the C-terminal NADPH binding site. In all cases, very pure protein was obtained (Figure 2, panel A), with the wild-type and mutant proteins migrating at the expected molecular masses in denaturing SDS−PAGE. The expression levels were ∼2 mg/L of *E. coli* culture for both the wild-type ($M_R = 135$ kDa) and the $\Delta^{52}$ mutant ($M_R = 129$ kDa), ∼2.5 mg/L for the $\Delta^{91}$ mutant ($M_R = 125$ kDa), and ∼1.5 mg/L for the $\Delta^{105}$ mutant ($M_R = 123$ kDa).

The NO formation activity (hemoglobin capture assay) of the $\Delta^{52}$ protein is ∼130 nmol $min^{-1}$ $mg^{-1}$ at 37 °C, a value

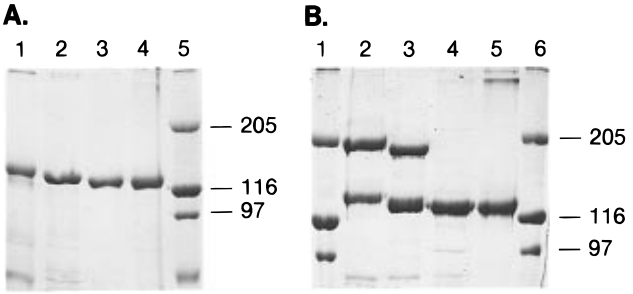


FIGURE 2: SDS−PAGE analysis of the purified, recombinant wild-type eNOS and the $\Delta^{52}$, $\Delta^{91}$, and $\Delta^{105}$ mutants under two sets of conditions. (A) SDS-denatured, boiled samples: lane 1, wild-type bovine eNOS ($M_R$ = 135 kDa); lane 2, $\Delta^{52}$ mutant ($M_R$ = 129 kDa); lane 3, $\Delta^{91}$ mutant ($M_R$ = 125 kDa); lane 4, $\Delta^{105}$ mutant ($M_R$ = 123 kDa); lane 5, molecular mass standards. (B) "Pseudo native" unboiled samples run at 4 °C: lanes 1 and 6, molecular mass standards; lane 2, wild-type bovine eNOS; lane 3, $\Delta^{52}$ mutant; lane 4, $\Delta^{91}$ mutant; lane 5, $\Delta^{105}$ mutant. Approximately 5 $\mu$g of protein was loaded per lane and the gels were stained with Coomassie blue.

similar to that for the wild-type protein (Rodríguez-Crespo et al., 1996). This mutant lacks the myristoylation site, the two palmitoylation sites, and the poly-Pro region that are present in eNOS but not in nNOS or iNOS. Myristoylation and palmitoylation are required for attachment of the protein to the membrane, and the poly-Pro region presumably functions as a linker between the lipid binding domain and the rest of the protein. Retention of full catalytic activity in the $\Delta^{52}$ mutant clearly establishes that these three regions are dispensable for catalytic activity and are only required for subcellular localization.

The $\Delta^{91}$ and $\Delta^{105}$ mutant proteins also produce NO, albeit at lower levels. The activity of $\Delta^{91}$ is ~25 nmol min$^{-1}$ mg$^{-1}$ at 37 °C, ~20% of the wild-type activity, and that of $\Delta^{105}$ is ~15 nmol min$^{-1}$ mg$^{-1}$, ~12% of the wild-type activity. The decrease in activity is not surprising, given that the truncation in $\Delta^{91}$ includes residues that are highly conserved among the various NOS isoforms, and in $\Delta^{105}$ the extended deletion includes two highly conserved cysteine residues (Cys-96 and Cys-101) (Figure 1). Previous reports have suggested that Cys-99 in human eNOS (Cys-101 of the bovine enzyme) is required for the efficient binding of $H_4B$ (Chen et al., 1995). However, the $\Delta^{105}$ mutant exhibited the same activity with a normal $H_4B$ concentration of 10 $\mu$M as it did with $H_4B$ concentrations up to 80 $\mu$M, in contrast to the report that a 10-fold higher concentration of $H_4B$ is required when Cys-99 is site specifically mutated to an alanine (Chen et al., 1995).

The catalytic activity of $\Delta^{91}$ and $\Delta^{105}$ is maximal when assayed immediately after purification and in the presence of 100 $\mu$M L-Arg (see Experimental Procedures). After a freeze−thaw cycle there is a significant loss of activity. Additionally, L-Arg must be added to the purified protein prior to storage at −75 °C to preserve the ability of the thawed protein to bind substrate. However, if the proteins are used immediately after purification and are maintained in the presence of 10 $\mu$M $H_4B$ and 100 $\mu$M L-Arg, they are stable for a period of at least 1 h.

To test whether the reductase domain of the expressed proteins is intact, the cytochrome c reduction activity of the $\Delta^{105}$ mutant, the truncated proteins with the lowest NO production activity, and the wild-type enzyme were compared. At 37 °C, the $\Delta^{105}$ mutant reduced cytochrome *c* at a rate of ~6 $\mu$mol min$^{-1}$ mg$^{-1}$ in the presence of CaM, a value essentially identical to that for the wild-type protein (3−5 $\mu$mol min$^{-1}$ mg$^{-1}$) under the same conditions (Rodríguez-Crespo et al., 1996). The rate of cytochrome *c* reduction was 5-fold lower for the $\Delta^{105}$ mutant, and 7-fold lower for the wild-type enzyme, in the absence of CaM.

*Monomer−Dimer Ratio.* SDS−PAGE at low temperature and FPLC were employed to determine the monomer−dimer equilibria of the wild-type protein and the three deletion mutants. $\Delta^{52}$ exhibits the same ~1:1 monomer−dimer ratio on SDS−PAGE as the wild-type enzyme (Figure 2B, lanes 2 and 3) (Rodríguez-Crespo et al., 1996). When $\Delta^{91}$ and $\Delta^{105}$ are run under identical conditions, the protein is found mostly in the monomeric state (Figure 2B, lanes 4 and 5). However, if these two mutants are allowed to stand at 4 °C immediately after purification in the absence of L-Arg and $H_4B$, aggregation occurs rapidly as indicated by the appearance of large molecular weight species (>dimers), some of which are so large as to be excluded from the running gel. The $\Delta^{91}$ and $\Delta^{105}$ protein aggregates suggest the presence of abnormal protein−protein contacts and indicate that in these two mutants the dimerization process is severely perturbed (see below).

FPLC analysis of the wild-type and truncated proteins indicates that the N-terminal deletions profoundly alter the monomer−dimer equilibrium (Table 1). Wild-type bovine eNOS appears primarily as a dimer with $V_e \approx 11$ mL; a minor monomer contribution is seen as a shoulder at $V_e \approx$ 12.6 mL (Figure 3). Protein aggregates also show up close to the void volume ($V_0$). Although $\Delta^{52}$ behaves very similarly to the wild-type protein on SDS−PAGE, FPLC analysis of the mutant shows a lower population of the dimer (Figure 3). The $\Delta^{91}$ and $\Delta^{105}$ mutants are similarly involved in a monomer−dimer equilibrium (Table 1), but additional larger aggregates are also observed (Figure 3). If the samples are analyzed immediately after purification, the contribution of higher order aggregates is smaller than if the samples are frozen and thawed, or allowed to stand at 4 °C. Already after 1 h at 4 °C, $\Delta^{91}$ and $\Delta^{105}$ are present only as large protein aggregates. Species of $\Delta^{91}$ and $\Delta^{105}$, eluting with longer retention times ($V_e$ >14 mL), are probably due to the existence of misfolded proteins (Figure 3) that are essentially absent in the case of the wild-type eNOS and its $\Delta^{52}$ mutant. It is important to note that these FPLC elution profiles are not affected by the presence or absence of L-Arg and $H_4B$.

Calibration of the FPLC column with a set of 7 globular proteins (Experimental Procedures) suggests that neither the monomer nor dimer of bovine eNOS behaves as a globular protein. The eNOS dimer ($V_e \approx 11$ mL) elutes immediately after apoferritin ($V_e \approx 10.7$ mL; 443 kDa), and the eNOS monomer ($V_e \approx 12.6$ mL) elutes very close to $\beta$-amylase ($V_e \approx 12.2$ mL; 200 kDa). Previous FPLC, sedimentation, and diffusion studies performed with nNOS by Mayer and co-workers as well as FPLC studies with human eNOS in our laboratory have provided similar evidence for elongated protein shapes (Rodríguez-Crespo & Ortiz de Montellano, 1996; Klatt et al., 1995, 1996).

*Spectroscopic Characterization.* The spectroscopic properties of the truncated eNOS proteins are compared with those of the wild-type enzyme in Figure 4. Since there is no $H_4B$ present in *E. coli*, it is possible to purify protein in the complete absence of the pterin cofactor (Rodríguez-Crespo et al., 1996). The spectrum of the purified ferric

Table 1: Properties of Wild-Type and Truncated Bovine eNOS

| | enzymatic activity (nmol $min^{-1}$ $mg^{-1}$) | monomer−dimer equilibrium | in absence of L-Arg and $H_4B$ | in presence of L-Arg and $H_4B$ |
|---|---|---|---|---|
| wild-type | ∼130 (100%) | mostly dimer | 400 nm (5cHS-6cLS) | 394 nm (5cHS) |
| $\Delta^{52}$ | ∼130 (100%) | mostly dimer | 400 nm (5cHS-6cLS) | 394 nm (5cHS) |
| $\Delta^{91}$ | ∼25 (20%) | monomers−dimers | 418 nm (6cLS) | 394 nm (5cHS-6cLS) |
| $\Delta^{105}$ | ∼15 (12%) | monomers−dimers | 418 nm (6cLS) | 394 nm (5cHS-6cLS) |

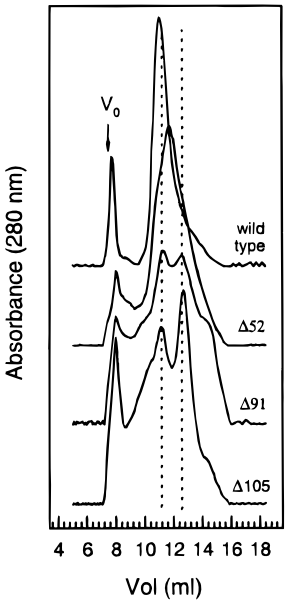


FIGURE 3: Gel filtration chromatography on a Superdex 200 HR column of wild-type bovine eNOS and the $\Delta^{52}$, $\Delta^{91}$, and $\Delta^{105}$ mutants. The dotted lines mark the approximate elution position of the dimeric (about 10.9 mL) and monomeric (about 12.6 mL) species. $V_0$ depicts the column void volume. The samples were run at ∼25 °C as detailed in the experimental Procedures.

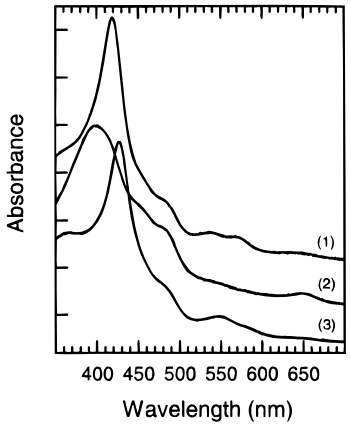


FIGURE 4: Absorption spectra of the recombinant eNOS proteins. Trace (1) shows the low-spin spectrum of either $\Delta^{91}$ or $\Delta^{105}$ as purified in the absence of L-Arg and $H_4B$. Trace 2 shows the spectrum of either wild-type eNOS or the $\Delta^{52}$ mutant purified in the absence of L-Arg and $H_4B$. Trace (3) shows wild-type bovine eNOS in the presence of 50 mM imidazole. The samples are in 10% glycerol, 50 mM Hepes, and 100 mM NaCl (pH 7.5).

$\Delta^{52}$ mutant in the absence of L-Arg and $H_4B$, with the characteristic broad maximum at 400 nm and flavin absorption maxima at ∼460 and 485 nm, is indistinguishable from that of the wild-type protein (Figure 4, trace 2). Binding of L-Arg to wild-type (Rodríguez-Crespo et al., 1996) and $\Delta^{52}$ sharpens the spectrum and causes the Soret maximum to shift from 400 to 395 nm, as expected from a low to high-spin transition (data not shown). The spectroscopic changes induced by binding of $H_4B$ to the $\Delta^{52}$ mutant (Table 1) are similar to those we previously reported for the wild-type protein (Rodríguez-Crespo et al., 1996). However, the spectra of the $\Delta^{91}$ and $\Delta^{105}$ mutants when purified without L-Arg and $H_4B$, with a sharp maximum at 418 nm and two very clear $\alpha/\beta$ bands at 570 and 535 nm (Figure 4, trace 1), are very different from that of the wild-type protein. Addition of imidazole to the wild-type protein in the absence of L-Arg produces a low-spin heme with a Soret band at 427 nm and a visible band at 550 nm (Figure 4, trace 3). This wild-type low-spin spectrum is distinct from the low-spin spectra obtained for the $\Delta^{91}$ and $\Delta^{105}$ mutants, probably because the sixth ligand differs in the two cases. The identity of the axial ligand in the $\Delta^{91}$ and $\Delta^{105}$ mutants is unknown. No spectral differences were observed when these mutants were titrated from pH 5.5 to 8.0 (data not shown), suggesting that the ligand may not be a water molecule.

To determine if the ligand in the $\Delta^{91}$ and $\Delta^{105}$ mutants is an imidazole introduced during elution of the proteins from the $Ni^{2+}$-NTA column, a calmodulin-Sepharose column was substituted as the first purification step. The absorption spectra of the resulting proteins still display the sharp peak at 418 nm, thus eliminating exogenous imidazole as the distal ligand in the two most severely truncated proteins. The integrity of the proximal thiolate iron ligand in all three mutants is confirmed by the observation of a normal 444 nm absorption maximum for the ferrous−CO complexes without the presence of a detectable 420 nm chromophore. This fact, together with a high heme to flavin absorbance ratio, supports the view that the deletions do not result in heme loss or altered heme binding.

When high concentrations of L-Arg are added to the $\Delta^{91}$ and $\Delta^{105}$ mutants, a low- to high-spin transition is observed (Figure 5A); more than 15 min are required to complete this spin-state shift. The binding of this natural substrate causes a decrease in the 418 nm maximum with a progressive increase at 398 nm, as well as an increase in absorption at 540 and 650 nm and a decrease at 570 nm (Figure 5A). When 10 $\mu$M $H_4B$ is added to the L-Arg-saturated $\Delta^{91}$ and $\Delta^{105}$ mutants, the spectral maximum shifts to 394 nm with a further decrease of the low-spin contribution (Figure 5B). Hence, the pterin cofactor is able to bind to these mutants to promote a low- to high-spin transition, as it does in the wild-type (Rodríguez-Crespo et al., 1996). An increase at ∼460 nm is also observed upon $H_4B$ binding to the L-Arg-saturated protein, a spectroscopic change not observed with L-Arg-saturated wild-type eNOS. The increase may result from coordination of DTT in a small subpopulation of the mutant protein, giving a bisthiolate complex (see below).

When $H_4B$ is added to the $\Delta^{91}$ and $\Delta^{105}$ mutants in the absence of L-Arg, the DTT present in the $H_4B$ solution coordinates to give a cysteinate−thiolate complex with absorption maxima at 374 and 461 nm (Figure 6 A) and a concomitant decrease in the absorbance at 418 nm. The same result is obtained if DTT is added without $H_4B$. DTT

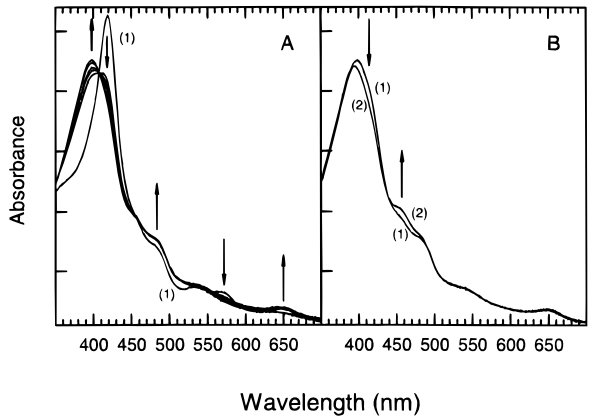


FIGURE 5: Absorption spectra of the $\Delta^{91}$ mutant upon sequential addition of L-Arg and $H_4B$. (A) Spectrum of the $\Delta^{91}$ mutant as purified in the absence of L-Arg and $H_4B$ (trace 1) to which 10 mM L-Arg was added in the absence of $H_4B$. Spectra were recorded every 3 min after the addition of L-Arg. The absorbance maximum of the final spectrum is at 398 nm; (B) Changes in the absorbance spectrum of the L-Arg saturated $\Delta^{91}$ mutant (i.e., final spectrum from panel A) due to addition of 10 $\mu$M $H_4B$. Absorption spectrum of $\Delta^{91}$ after preincubation at 25 °C for 20 min with saturating concentrations of L-Arg (trace 1), and the spectrum recorded immediately after adding $H_4B$ (trace 2). The final absorbance maximum of the L-Arg- and $H_4B$-bound protein is at 394 nm. The arrows indicate the direction of the spectral changes. The protein solutions were in 10% glycerol, 50 mM Hepes, and 100 mM NaCl (pH 7.5). The 10 mM $H_4B$ stock solution was prepared in 100 mM DTT. Identical results are observed with the $\Delta^{105}$ mutant.

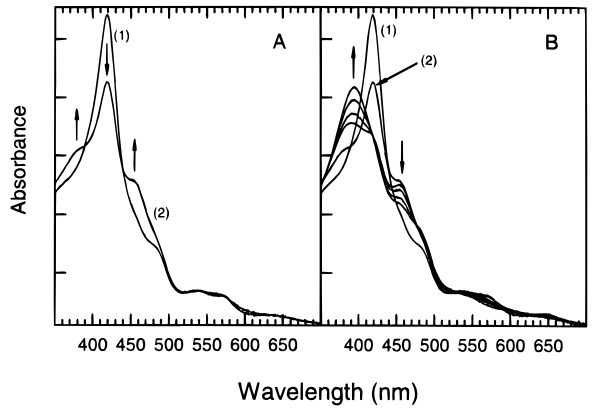


FIGURE 6: Absorption spectra of the $\Delta^{91}$ mutant upon sequential addition of $H_4B$ and L-Arg. (A) Spectra of the $\Delta^{91}$ mutant purified in the absence of L-Arg and $H_4B$ (trace 1) and after the addition of 10 $\mu$M $H_4B$ and 100 $\mu$M DTT (no L-Arg present) (trace 2). (B) Spectra showing the effect of 10 mM L-Arg on the $H_4B$-saturated (10 $\mu$M $H_4B$) $\Delta^{91}$ mutant (trace 2). L-Arg was added to $\Delta^{91}$ after preincubation at 25 °C for 5 min with 10 $\mu$M $H_4B$ (trace 1) and the absorption spectrum was recorded every 3 min after addition of the L-Arg. The absorbance maximum of the final spectrum is at 394 nm. The arrows indicate the direction of the spectral changes. The protein solutions were in 10% glycerol, 50 mM Hepes, and 100 mM NaCl (pH 7.5). The 10 mM $H_4B$ stock solution was prepared in 100 mM DTT. Identical results were observed with the $\Delta^{105}$ mutant.

does not bind, however, in the presence of high L-Arg concentrations. In $P450_{cam}$, coordination of DTT results in spectral changes at 374 nm ($\epsilon$ = 67 mM cm$^{-1}$), 461 nm ($\epsilon$ = 57 mM cm$^{-1}$) and 557 nm ($\epsilon$ = 11.6 mM cm$^{-1}$), (Dawson et al., 1982), essentially as is observed for the $\Delta^{91}$ and $\Delta^{105}$ eNOS mutants. DTT coordination in the mutants points to a major alteration on the distal side of the heme because DTT does not coordinate in the wild-type enzyme. Binding of DTT has been used previously as a probe of the

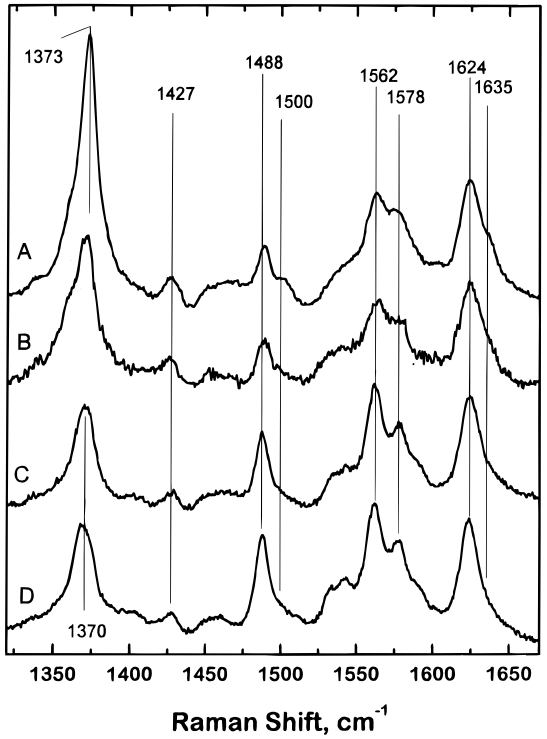


FIGURE 7: Resonance Raman spectra in the high-frequency region of wild-type eNOS under different conditions. From top to bottom: in the absence of L-Arg and $H_4B$ (A); in the presence of 10 $\mu$M $H_4B$ and no L-Arg (B); in the presence of 10 mM L-Arg and no $H_4B$ (C); in the presence of both 10 $\mu$M $H_4B$ and 10 mM L-Arg (D). Resonance Raman spectra were obtained at room temperature with 413 nm laser excitation as indicated in the Experimental Procedures.

dimerization of the iNOS heme domain (Ghosh et al., 1996). Dimeric iNOS, which does not bind DTT, is dissociated in 5 M urea to monomers that do bind DTT. Since the $\Delta^{91}$ and $\Delta^{105}$ mutants exhibit impaired dimer formation, it follows that it is the monomeric population of the protein that coordinates DTT. When 10 mM L-Arg is added to the $H_4B$-saturated solution, DTT is slowly displaced, as shown by an increase in the absorption at 394 nm and disappearance of the maxima at 418 and 461 nm (Figure 6B). Thus, binding of L-Arg near the heme displaces the DTT with concomitant formation of a typical high-spin spectrum. A mixture of 5cHS and 6cLS species has also been observed by resonance Raman spectroscopy in $H_4B$-free nNOS (Wang et al., 1995).

Upon addition of freshly prepared, DTT-free $H_4B$ (10 $\mu$M final concentration) to the $\Delta^{91}$ and $\Delta^{105}$ mutants, a small decrease is observed at 420 nm similar to that reported for wild-type eNOS (Rodríguez-Crespo et al., 1996). Whereas the L-Arg induced spectral changes were slow, the effect of $H_4B$ is almost immediate at 15 °C.

*Resonance Raman Characterization.* The nature of the heme pocket in wild-type eNOS and its $\Delta^{91}$ and $\Delta^{105}$ mutants was also studied by RR spectroscopy. Figure 7 compares the high-frequency region of the wild-type eNOS spectrum obtained in the absence of $H_4B$ and L-Arg (trace A) and after the addition of $H_4B$ only (trace B), L-Arg only (trace C), or both $H_4B$ and L-Arg (trace D). The RR spectrum of $H_4B$-free, L-Arg-free wild-type eNOS is indicative of a mixture of pentacoordinate high-spin (5cHS) and hexacoordinate low-spin (6cLS) hemes (Table 1). The vibrational modes characteristic of the 5cHS species are $\nu_3$ at 1488 cm$^{-1}$ and

$\nu_2$ at 1562 $cm^{-1}$; the corresponding RR bands for the 6cLS species are at 1500 and 1578 $cm^{-1}$, respectively.

Upon addition of $H_4B$ and L-Arg, the 6cLS population is fully converted to 5cHS, as revealed by the presence of a single $\nu_3$ component at 1488 $cm^{-1}$, and is confirmed by other RR spectral changes (Figure 7D). The $\nu_4$ mode shifts from 1373 $cm^{-1}$, an unresolved combination of the frequencies of the 5cHS (1370 $cm^{-1}$) and the 6cLS (1375 $cm^{-1}$) species, to 1370 $cm^{-1}$ consistent with a pure HS spectrum.[2] In the $\nu_2$ region, the 1562/1578 $cm^{-1}$ intensity ratio increases in favor of the 5cHS component, but significant RR intensity is preserved at 1577 $cm^{-1}$. However, other heme skeletal vibrational modes such as $\nu_{19}$ also occur in this region (Wang et al., 1995). The 6cLS RR feature at 1635 $cm^{-1}$ due to $\nu_{10}$ is also eliminated.

Binding of L-Arg in the absence of $H_4B$ results in a loss of the hexacoordinate low-spin markers at 1500 ($\nu_3$) and 1635 ($\nu_{10}$) $cm^{-1}$ (Figure 7C). The effect of L-Arg alone is essentially identical to that observed for L-Arg plus $H_4B$ as described above, and suggests that the substrate plays the major role in the conversion.

In keeping with this observation, addition of $H_4B$ in the absence of L-Arg leads to only subtle changes in the intensities of the spin-state markers at 1500 ($\nu_3$) and 1635 ($\nu_{10}$) $cm^{-1}$ (Figure 7B). These RR results are fully consistent with the optical absorption data on eNOS described above. A similar low-spin to high-spin conversion upon addition of $H_4B$ has also been observed by RR spectroscopy in the neuronal NOS isoform (Wang et al., 1995). We previously characterized the low- to high-spin transition induced upon $H_4B$ binding in wild-type eNOS by optical difference spectroscopy (Rodríguez-Crespo et al., 1996). Our recent observations that $H_4B$ binding induces a more restricted access of phenylhydrazines to the region over the heme pyrrole ring D (Gerber et al., 1997) indicates that, unlike L-Arg, the pterin cofactor is not directly positioned over the heme iron but is still able to affect the heme electronic environment.

In contrast to the wild-type enzyme, the $H_4B$-free, L-Arg-free preparations of the eNOS mutants $\Delta^{91}$ and $\Delta^{105}$ have RR spectra typical of pure 6cLS hemes with $\nu_3$ at 1501 $cm^{-1}$ and $\nu_{10}$ at 1636 $cm^{-1}$ (Figure 8, traces A and B). Addition of $H_4B$ and L-Arg to these mutants results in a dramatic conversion to 5cHS species with $\nu_3$ at 1488 $cm^{-1}$, $\nu_2$ at 1562 $cm^{-1}$, and loss of $\nu_{10}$. Nonetheless, the $H_4B$ and L-Arg saturated $\Delta^{91}$ and $\Delta^{105}$ mutants still exhibit a spin-state mixture as judged by the RR data. The optical absorption spectra for $\Delta^{91}$ and $\Delta^{105}$ under the same conditions (Figure 5) failed to reveal the residual LS species, and hence, attests to the sensitivity of the RR technique. By comparison, saturating levels of $H_4B$ and L-Arg added to wild-type enzyme led to complete conversion to the 5cHS form (Figure 7, Table 1).

[2] In high-spin ferric NOS samples containing substrate, unusual decreases are observed for the intensity of the oxidation-state marker band, $\nu_4$, typically one of the most intense RR bands. The effect is also noted in the presence of $H_4B$, but is more pronounced for L-Arg. Although the origin of this intensity change is unknown, it is likely related to the presence of the cysteinyl thiolate ligand; a similarly diminished $\nu_4$ intensity can be seen in oxidized, substrate-bound cytochrome P-$450_{cam}$ (Wells et al, 1992).

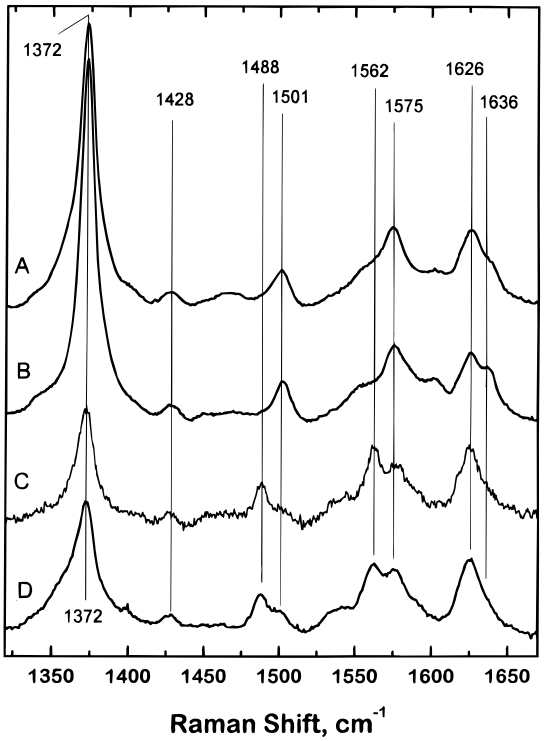


FIGURE 8: Resonance Raman spectra in the high frequency region of N-terminal deletion mutants $\Delta^{91}$ and $\Delta^{105}$ under different conditions. From top to bottom: deletion mutant $\Delta^{91}$ in the absence of L-Arg and $H_4B$ (A); deletion mutant $\Delta^{105}$ in the absence of L-Arg and $H_4B$ (B); deletion mutant $\Delta^{91}$ in the presence of both 10 mM L-Arg and 10 $\mu$M $H_4B$ (C); deletion mutant $\Delta^{105}$ in the presence of both 10 mM L-Arg and 10 $\mu$M $H_4B$ (D). Resonance Raman spectra were obtained at room temperature with 413 nm laser excitation as indicated in the Experimental Procedures.

## DISCUSSION

Deletions from the C-terminus of mouse iNOS have demonstrated that elimination of the last 10 amino acids produces an inactive protein that dimerizes, binds heme and CaM, but is defective in its ability to bind NADPH (Xie et al., 1994). N-terminal deletions of conserved residues in the heme domain of NOS have not been reported.

Cloning and expression of the nNOS heme domain (McMillan & Masters, 1995) and proteolytic cleavage of iNOS into its component domains (Ghosh & Stuehr, 1995) have been used to establish that the N-terminal half of the polypeptide chain is involved in L-Arg and $H_4B$ binding. It has also been shown by expression of the individual iNOS domains that the heme domain can dimerize in solution, whereas the reductase domain remains monomeric (Ghosh & Stuehr, 1995). Unpublished results from this laboratory indicate that the heme domains of rat neuronal and bovine endothelial NOS can also associate into homodimers. This behavior strongly suggests that most, and possibly all, of the interactions required for dimer formation involve residues located in the N-terminal half of the protein, but the specific residues responsible for dimer formation have not been identified. In this work, three N-terminal deletion mutants of bovine eNOS, each of increasing length, have been constructed to investigate the role of the N-terminal residues on enzyme activity, protein dimerization, and the binding of L-Arg and $H_4B$ (Table 1).

Deletion of the first 52 amino acids of bovine eNOS yields a truncated protein ($\Delta^{52}$) that retains most of the structural

properties of the wild-type enzyme and exhibits full catalytic activity. Since the regions involved in subcellular localization have been deleted in the truncated protein, it is clear that myristoylation and palmitoylation are not required for normal enzyme turnover. In addition, the finding that deletion of the poly-Pro region in the N-terminus does not affect the integrity or activity of the protein supports the assignment of a linker function to this polypeptide stretch.

When the N-terminal deletions are extended to positions 91 and 105 (Figure 1), profound alterations are observed in the distal heme site, including the presence of a hexacoordinated low-spin heme iron atom. This contrasts with the wild-type and $\Delta^{52}$ proteins, in which the iron in the resting state is mostly pentacoordinated high-spin. However, both the $\Delta^{91}$ and $\Delta^{105}$ mutants retain the ability to bind L-Arg and $H_4B$, as demonstrated by the low- to high-spin transitions observed when either of these molecules is bound. In addition to the spectroscopic changes, FPLC and low-temperature SDS−PAGE indicate that the monomer−dimer equilibrium is severely altered in the $\Delta^{91}$ mutant, and to an even larger extent in the $\Delta^{105}$ mutant, although a significant population of the dimers of both mutants remains. The change in the dimer population is due to specific alterations of the protein at the dimer interface rather than misfolding of the protein because the thiolate ligand to the heme, a very sensitive indicator of the structure of the protein in the vicinity of the heme, is retained. Evidence that the reductase domain of the protein is also intact is provided by the finding that the cytochrome *c* reductase activity of the $\Delta^{105}$ mutant is the same as that of the wild-type protein. Thus, although the protein is sensitive to aggregate formation and denaturation, both domains of the fraction of the protein that is catalytically competent appear to be properly folded.

Studies of porcine nNOS by Mayer and co-workers (Klatt et al., 1995) previously suggested that substrate binding may occur at the interface between the two monomers. This conclusion was based on the observation that both L-Arg and $H_4B$ stabilized the protein dimer against SDS-induced monomerization. Although we have not found that either L-Arg or $H_4B$ stabilizes the dimer of bovine eNOS (Rodríguez-Crespo et al., 1996), it is nevertheless possible that substrates bind to eNOS at the interface between the two protein monomers. In fact, our finding that peptide deletions that perturb dimer formation also alter the binding of L-Arg is consistent with localization of the substrate binding site at the monomer−monomer interface. The spectroscopically demonstrated binding of DTT to the $\Delta^{91}$ and $\Delta^{105}$, but not $\Delta^{52}$, mutants is consistent with dimer-dependent assembly of the intact substrate binding site. The lower catalytic activity of the $\Delta^{91}$ and $\Delta^{105}$ mutants is readily rationalized by the decrease in the dimer population of these proteins and by the associated impairment of substrate binding.

Sequence homology between amino acid hydroxylases and mouse iNOS suggests that residues 448−480 are involved in $H_4B$ binding (Cho et al., 1995). This region is highly conserved among the various NOS isoforms. Site-directed mutants with substitutions in this region are reportedly defective in both $H_4B$ binding and dimer formation and exhibit impaired NO production (Cho et al., 1995). An alternate, widely separated $H_4B$ binding site has been proposed based on a Cys-99 → Ala mutation in human eNOS (Cys-101 in bovine eNOS). This mutant had a low heme content and exhibited enzymatic activity only with 10-fold higher concentrations of $H_4B$ than required for catalytic turnover of the wild-type enzyme (Chen et al., 1995). In our $\Delta^{105}$ mutant, the two highly conserved cysteine residues, Cys-96 and Cys-101, have been eliminated altogether. The $\Delta^{105}$ mutant nevertheless binds $H_4B$, as indicated by the observation in difference spectroscopy of a clear decrease in the 420 nm absorption upon the addition of $H_4B$ (data not shown). Furthermore, the maximum catalytic activity of the protein is obtained with a normal 10 $\mu$M concentration of $H_4B$, and is not increased by higher concentrations of this cofactor. The reason for the discrepancy between the present results and the earlier site-specific mutagenesis studies is unclear, although the spectroscopic data reported for the C99A mutant used in the earlier studies suggests that the protein was not of high quality. Our results suggest that the role of Cys-101 in the binding of $H_4B$ is limited, at best, and indicate that the effects of the truncations on L-Arg binding and dimer formation probably account for the diminished NO synthetic activities of both the $\Delta^{91}$ and $\Delta^{105}$ mutant.

Two recent papers describe alternative splicing of the nNOS gene to give natural nNOS variants with N-terminal deletions. One of them, a human testis-specific protein known as TnNOS, is missing the first 336 N-terminal amino acids (Wang et al., 1997). This protein is reported to retain at least some catalytic activity. The other two, known as $nNOS_\beta$ and $nNOS_\gamma$, are mouse brain proteins from which the first 236 and 330 N-terminal amino acids, respectively, have been deleted (Brenman et al., 1996). Mouse brain $nNOS_\beta$ is reported to be active, but $nNOS_\gamma$ is reportedly inactive. Interestingly, the truncations in human TnNOS and mouse $NOS_\gamma$ occur at positions equivalent to Leu-102 in bovine eNOS. The two natural truncated proteins are thus of almost exactly the same length as the $\Delta^{105}$ truncated eNOS protein described here. As the activities of the endogenous proteins were only determined in crude cell extracts after expression in mammalian cells, it is not possible to make precise comparisons of the activities and properties of the endogenous proteins with the eNOS $\Delta^{105}$ construct. Nevertheless, our data on the $\Delta^{105}$ protein clearly show that a NOS of that length retains many of the structural features of the intact, full-length protein as well as part of its catalytic activity. The results also suggest that the endogenous truncated proteins will be less stable than the full length nNOS, particularly in the absence of $H_4B$ and L-Arg.

In sum, deletion of 52 amino acids from the amino terminus of bovine eNOS yields a protein with properties very similar to those of the wild-type enzyme despite the loss of sites involved in lipid binding and enzyme targeting. In contrast, deletion of 91 and 105 amino acids yields proteins with altered spectroscopic, iron coordination, substrate binding, and dimerization properties, but which still exhibit 20 and 12%, respectively. of the activity of the wild-type enzyme. The first 52 amino acids thus are irrelevant for the catalytic action of the enzyme, whereas the polypeptide chain between residues 52 and 105 includes amino acids that facilitate, but are not absolutely essential, for protein dimerization, $H_4B$ binding, or maintenance of a catalytically functional active site architecture.

## REFERENCES

Bredt, D. S., & Snyder, S. H. (1994) *Annu. Rev. Biochem. 63*, 175−195.

Bredt, D. S., Hwang, P. M., Glatt, C. E., Lowenstein, C., Reed, R. R., & Snyder, S. H. (1991) *Nature 351*, 714−718.
Brenman, J. E., Chao, D. S., Xia, H., Aldape, K., & Bredt, D. S. (1995) *Cell 82*, 743−752.
Brenman, J. E., Chao, D. S., Gee, S. H., McGee, A. W., Craven, S. E., Santillano, D. R., Wu, Z., Huang, F., Xia, H., Peters, M. F., Froehner, S. C., & Bredt, D. S. (1996) *Cell 84*, 757−767.
Busconi, L., & Michel, T. (1993) *J. Biol. Chem. 268*, 8410−8413.
Chen, P.-F., Tsai, A.-L., & Wu, K. K. (1995) *Biochem. Biophys. Res. Commun. 215*, 1119−1129.
Cho, H. J., Martin, E., Xie, Q-W., Sassa, S., & Nathan, C. (1995) *Proc. Natl. Acad. Sci. U.S.A. 92*, 11514−11518.
Dawson, J. H., Andersson, L. A., & Sono, M. (1982) *J. Biol. Chem. 257*, 3606−3617.
Gerber, N. C., & Ortiz de Montellano, P. R. (1995) *J. Biol. Chem. 270*, 17791−17796.
Gerber, N. C., Rodriguez-Crespo, I., Nishida, C. R., & Ortiz de Montellano, P. R. (1997) *J. Biol. Chem*. 272, 6285−6290.
Ghosh, D. K., & Stuehr, D. J. (1995) *Biochemistry 34*, 801−807.
Ghosh, D. K., Abu-Soud, H. M., & Stuehr, D. J. (1996) *Biochemistry 35*, 1444−1449.
Griffith, O., & Stuehr, D. J. (1995) *Annu. Rev. Physiol. 57*, 707−736.
Klatt, P., Schidt, K., Lehner, D., Glatter, O., Bächinger, H. P., & Mayer, B. (1995) *EMBO J. 14*, 3687−3695.
Klatt, P., Pfeiffer, S., List, B. M., Lehner, D., Glatter, O., Bächinger, H. P., Werner, E. R., Schmidt, K., & Mayer, B. (1996) *J. Biol. Chem. 271*, 7336−7342.
Knowles, R. G., & Moncada, S. (1994) *Biochem. J. 298*, 249−258.
Lin, A. W., Chang, C. C., & McCormick, C. C. (1996) *J. Biol. Chem. 271*, 11911−11919.
Liu, J., García-Cardeña, G., & Sessa, W. C. (1996) *Biochemistry, 35*, 13277−13281.
Loehr, T. M., & Sanders-Loehr, J. (1993) *Methods Enzymol. 226*, 431−470.
Marletta, M. A. (1994) *Cell 78*, 927−930.
Masters, B. S. S. (1994) *Annu. Rev. Nutr. 14*, 131−145.
McMillan, K., & Masters, B. S. S. (1995) *Biochemistry 34*, 3686−3693.
Regulski, M., & Tully, T. (1995) *Proc. Natl. Acad. Sci. U.S.A. 92*, 9072−9076.
Ringheim, G. E., & Pan, J. (1995) *Biochem. Biophys. Res. Commun. 210*, 711−716.
Rodríguez-Crespo, I., & Ortiz de Montellano, P. R. (1996) *Arch. Biochem. Biophys. 336*, 151−156.
Rodríguez-Crespo, I., Gerber, N. C., & Ortiz de Montellano, P. R. (1996) *J. Biol. Chem. 271*, 11462−11467.
Sessa, W. C., Harrison, J. K., Barber, C. M., Zeng, D., Durieux, M. E., D'Angelo, D. D., Lynch, K. R., & Peach, M. J. (1992) *J. Biol. Chem. 267*, 15274−15276.
Sessa, W. C., Barber, C. M., & Lynch, K. R. (1993) *Circ. Res. 72*, 921−924.
Shaul, P. W., Smart, E. J., Robinson, L., German Z., Yuhanna, I. S., Ying, Y., Anderson, R. G. W., & Michel, T. (1996) *J. Biol. Chem. 271*, 6518−6522.
Wang, J., Stuehr, D. J., & Rousseau, D. L. (1995) *Biochemistry 34*, 7080−7087.
Wang, Y., Goligorsky, M. S., Lin, M., Wilcox, J. N., & Marsden, P. A. (1997) *J. Biol. Chem. 272*, 11392−11401.
Wells, A. V., Li, P., Champion, P. M., Martinis, S. A., & Sligar, S. G. (1992) *Biochemistry 31*, 4384−4393
Xie, Q.-W., Cho, H. J., Calaycay, J., Mumford, R. A., Swiderek, K., Lee, T. D., Ding, A., Troso, T., & Nathan, C. (1992) *Science 256*, 225−228.
Xie, Q.-W., Cho, H. J., Kashiwabara, Y., Baum, M., Weidner, J. R., Elliston, K., Mumford, R., & Nathan, C. (1994) *J. Biol. Chem. 269*, 28500−28505.

BI970192J